

Parity breaking reshapes black hole spectral dynamics

Han-Wen Hu^{1,2,*}, Chen Lan^{3,†} and Zong-Kuan Guo^{1,2,4‡}

¹*Institute of Theoretical Physics, Chinese Academy of Sciences, P.O. Box 2735, Beijing 100190, China*

²*School of Physical Sciences, University of Chinese Academy of Sciences, No.19A Yuquan Road, Beijing 100049, China*

³*Department of Physics, Yantai University, 30 Qingquan Road, Yantai 264005, China and*

⁴*School of Fundamental Physics and Mathematical Sciences, Hangzhou Institute for Advanced Study, University of Chinese Academy of Sciences, Hangzhou 310024, China*

We propose a dynamical amplification mechanism for detecting symmetry breaking in black holes through environmentally driven spectral instabilities of quasinormal modes. Focusing on dynamical Chern-Simons gravity as a paradigm for parity violation, we perturb the Schwarzschild background with a localized potential bump. Our analysis reveals three distinctive phenomena absent in general relativity: 1) topological reconnections of mode branches, 2) counterintuitive mode stabilization that delays overtaking transitions, and 3) scalar mode dominance emerging at intermediate coupling strengths. These dynamical features amplify weak static splittings into observable signatures, establishing a connection between gravitational symmetry breaking and non-Hermitian spectral physics. Our framework provides new pathways for testing modified gravity theories through gravitational wave observations.

Introduction. Symmetries are cornerstones of general relativity (GR). For instance, the parity symmetry of Schwarzschild spacetime directly leads to the isospectrality of its gravitational perturbation spectrum: axial and polar perturbations share identical quasinormal mode (QNM) spectra [1–5]. However, numerous beyond-standard-model (BSM) gravity theories—whether inspired by string theory or quantum gravity—predict the breaking of fundamental symmetries [6–11]. Detecting such symmetry breaking is a core goal of gravitational wave astronomy [12–16].

The challenge lies in the fact that these breaking effects in static black hole (BH) backgrounds are typically weak, for example, only causing minor static splittings between axial and polar spectra that are hard to resolve at current observational precision [6, 8].

A key insight is that BHs are not isolated Hermitian systems; they are open, dissipative systems whose QNM spectra are fundamentally non-Hermitian [5, 17–19]. Recent studies show that this non-Hermitian nature makes QNM spectra extremely sensitive to tiny external perturbations (e.g., “dirty” astrophysical environments) [18–23]. This sensitivity can manifest as dramatic “spectral instabilities”, where QNM overtones “overtake” the fundamental mode, leading to topological mutations in the ringdown signal [21].

In this Letter, we propose using this environment-driven spectral instability as a dynamical amplifier to probe fundamental symmetry breaking. Our core hypothesis is that if a BSM theory breaks an underlying GR symmetry, such as parity, it will alter the non-Hermitian topological structure of the QNM spectrum, thereby significantly and observably changing the BH’s dynamical response to environmental perturbations. To validate this framework, we use dynamical Chern-Simons (dCS) gravity as a paradigmatic example of parity breaking [11, 24–28]. This theory breaks isospectrality via a scalar

field, with breaking strength controlled by $1/\beta$ ($\beta \rightarrow \infty$ recovers GR) [29]. We simulate environmental perturbations by introducing a localized bump [21, 30],¹ and systematically track the QNM spectrum’s evolution in the complex plane. Specifically, we report three distinctive signatures: topological reconnections of mode trajectories indicating non-Hermitian phase transitions; a counterintuitive stabilization of the gravitational mode by strong symmetry breaking; and a scalar mode dominance at intermediate couplings, which is impossible in GR.

Our findings directly link symmetry breaking in gravity to frontiers in non-Hermitian physics. The mode topological reconnection echoes exceptional point (EP) behaviors observed in Kerr BHs [31, 32], PT-symmetric waveguides [33, 34], and quantum tunneling [35–37]. More importantly, the strong dependence of the critical point a_{crit} on the symmetry-breaking parameter β transforms a weak, static spectral splitting into an amplified dynamical feature detectable by LIGO/Virgo or LISA. This framework not only provides new avenues to constrain dCS gravity but also opens a general path to test other fundamental symmetries (such as Lorentz symmetry [16, 38–40]) using BH non-Hermitian dynamics.

Parity Violating Model. We utilize dCS gravity as a paradigmatic theory for parity violation. The dCS action is given by [24, 29, 41]

$$S_{\text{dCS}} = \int d^4x \sqrt{-g} \left[R + \frac{\alpha}{8} \phi(x) \varepsilon^{\mu\nu\rho\sigma} R^\alpha_{\beta\mu\nu} R^\beta_{\alpha\rho\sigma} - \frac{\beta}{2} \partial_\mu \phi \partial^\mu \phi \right], \quad (1)$$

¹ Such a localized bump has been shown to effectively mimic astrophysical environmental effects and is particularly suited to probe near-horizon to far-region physics.

here we adopt the units where $c = 1$, $G = 1/8\pi$, i.e. $\kappa = 1$. The background spacetime remains the standard Schwarzschild metric, $ds^2 = -f(r)dt^2 + f^{-1}(r)dr^2 + r^2d\Omega^2$ with $f(r) = 1 - 2M/r$. Following standard conventions, we set $\alpha = 1$. The effective coupling strength is characterized by $1/\beta$; the $\beta \rightarrow \infty$ limit recovers GR, while small β signifies strong symmetry-breaking.

Parity breaking manifests at the perturbative level. While the polar sector perturbations remain governed by the Zerilli equation [24], the axial gravitational perturbation (Ψ) becomes coupled with the dCS scalar field perturbation (Θ). This yields the coupled wave equations [24]

$$\frac{d^2\Psi}{dr_*^2} + \left[\omega^2 - f \left(\frac{l(l+1)}{r^2} - \frac{6M}{r^3} \right) \right] \Psi = \frac{6M}{r^5} f \Theta, \quad (2a)$$

$$\frac{d^2\Theta}{dr_*^2} + \left\{ \omega^2 - f \left[\frac{l(l+1)}{r^2} \left(1 + \frac{36M^2}{r^6\beta} \right) + \frac{2M}{r^3} \right] \right\} \Theta = f \frac{(l+2)!}{(l-2)!} \frac{6M}{r^5\beta} \Psi, \quad (2b)$$

where r_* is the tortoise coordinates, $dr_* \equiv dr/f(r)$. The functions Ψ and Θ are derived from the Regge-Wheeler function and the scalar field expansion $\delta\phi = \frac{\Theta(r)}{r} Y^{lm}(\theta, \varphi) e^{-i\omega t}$, respectively.

To probe the system's dynamical response, we introduce a localized Pöschl-Teller bump to the gravitational potentials,

$$V_{\text{eff}} = V_{\text{Z/RW}} + V_{\text{bump}}, \quad V_{\text{bump}} = \epsilon \text{sech}^2(r_* - a). \quad (3)$$

This bump, characterized by amplitude ϵ and position a , simulates environmental effects or unknown physics [42, 43]. In our numerical calculations of next section, we fix $M = 1$, $l = 2$, and $\epsilon = 10^{-2}$. We then systematically track the QNM frequencies in the complex plane as the position of bump a is varied, moving away from the potential peak (near $r_* \simeq 1.614$). Our choice of amplitude $\epsilon = 10^{-2}$ is a deliberate strategy to ensure numerical tractability. As established in Ref. [21], the critical position a_{crit} for instability is inversely related to ϵ , cf. Fig. 2 of that work. A physically plausible, smaller ϵ would simply push the same critical phenomena to numerically challenging large distances. We therefore use $\epsilon = 10^{-2}$ to bring the relevant dynamics into our reliable computational domain, without loss of generality for the physical effects under investigation.

Spectral Topology. Based on the theoretical framework established in the previous section, this section presents the key numerical results regarding the effect of symmetry breaking on the stability of the QNM spectrum. We employ the shooting method to solve the corresponding QNM eigenfrequencies ω_n of the polar Zerilli equation and the axial coupled equations Eq. (2) after the inclusion of the bump potential. Specifically, this method imposes pure ingoing wave conditions at the event horizon and pure outgoing waves at spatial infinity, with the latter enforced via a numerical cutoff. The complex frequencies are found using Mathematica's `FindRoot` function.

We confirmed that all key phenomena discussed below achieving residuals of 10^{-6} or smaller.

To explore these effects, frequencies are computed for symmetry-breaking parameters $\beta = 0.1, 1$ and 1000 , alongside the polar sector as a minimally-broken control case. The analysis here will systematically trace how the quasinormal frequencies ω_n respond to the bump position a and the parameter β in the complex frequency space. The focus will be on several key phenomena co-induced by symmetry breaking and perturbation, including the shift of quasinormal frequencies, the critical threshold a_{crit} for the overtaking of the fundamental mode, and the deviation of the polar and axial QNM spectra of fundamental mode of gravitational perturbations in the vacuum case from the vacuum mode $\omega(0)$, defined as $\Delta\omega = \omega(\epsilon, a) - \omega(0)$.

Fig. 1 reveals the QNM migration trajectories in the complex frequency plane for $\beta = 0.1, 1$ and 1000 , analogous to the GR study of spectral instabilities. In each panel of Fig. 1, the gray lines trace the migration paths of the vacuum QNMs, while the red line tracks the migration of the dominant mode ϖ , i.e., the mode with the smallest negative imaginary part. For weak breaking $\beta = 1000$, the trajectories closely mirror those in GR. All gray migration paths of QNMs are nearly identical to those of the polar sector. This coincides with our physical intuition, in the $\beta \rightarrow \infty$ limit, the axial sector recovers GR's isospectrality [24]. At this point, the scalar modes hardly couple with the gravitational modes. Specifically in the complex frequency space, the migration path of each scalar mode starts from a vortex and quickly terminates in another vortex. They are completely separated from the migration paths of the gravitational modes, as shown in the panel(c) of Fig. 1.

As symmetry breaking intensifies, the paths deviate markedly. We observe a series of critical phenomena where the topological connectivity of the QNM trajectories undergoes fundamental reconnections. This is first

seen by comparing the macro-scale spectrum at $\beta = 1000$ (Panel (c) of Fig. 1) with the spectrum at $\beta = 1$ (Panel (a) of Fig. 1). At high β , we focus on two distinct, topologically separate curves: a S-shaped curve containing both vortices corresponds the dCS scalar mode and a simple upper curve corresponds to a GR overtone. At $\beta = 1$, however, the morphology and relative positions of these two curves have significantly changed. This implies a critical topological transition must occur within this interval. To locate this critical event, we performed a fine scan of parameter β , detailed in Fig. 2. At $\beta = 5$ (Panel(b) of Fig. 2), the spectrum consists of at least two topologically distinct curves: an upper simple curve (henceforth curve A) and a lower, S-shaped composite curve containing two vortices (henceforth curve B). As β crosses the critical value and reaches $\beta = 4$ (Panel(a) of Fig. 2), a reconnection occurs: the first part of curve A now connects to the second part of curve B, while the first part of curve B connects to the second part of curve A. This abrupt change in the physical topology of the solution space is the curve merging (or, reconnection) phenomenon, and it represents the mechanism for the macro-scale transition observed in Fig. 1. This can be viewed as a phase transition in the spectrum, driven by coupling strength.

This reconnection is a hallmark of the system's non-Hermitian nature. The dCS coupling allows for EPs, where modes coalesce [31]; traversing an EPs forces the coupled quasi-gravitational and quasi-scalar modes to “swap identities”, which manifests as the observed discontinuity. One can deduce that a similar reconnection event occurs by comparing panel (a) and panel (b) in Fig. 1.

By constructing a non-Hermitian effective Hamiltonian projected onto the unperturbed subspace (details in SM), we derive the resonance condition for topological reconnection

$$[\Omega_g^2(a) - \Omega_s^2(\beta)]^2 + 4\kappa_{sg}(\beta)\kappa_{gs} = 0, \quad (4)$$

where $\Omega_g^2(a)$ and $\Omega_s^2(\beta)$ represent the effective frequencies of the gravitational and scalar modes, respectively. The off-diagonal terms κ_{gs} and $\kappa_{sg}(\beta)$ characterize the non-Hermitian coupling strength between the two sectors. Physically, an EP emerges when the squared frequency detuning is exactly compensated by the coupling product. Varying β tunes the scalar sector into this critical resonance with the gravitational spectrum, forcing the eigenmodes to coalesce.

Quantitatively, a core discovery comes from the critical position for mode overtaking, a_{crit} —the value of a at which the first discontinuous jump in the dominant mode ϖ occurs. We treat the polar sector as GR baseline, it yields an overtaking threshold of $a_{\text{crit}}^{\text{polar}} \simeq 15$. However, the stability of the axial sector shows a clear dependence on the breaking strength: weak breaking ($\beta = 1000$) yields an axial threshold $a_{\text{crit}} \simeq 15$, perfectly converging to the

GR/polar baseline; intermediate breaking ($\beta = 1$) postpones the threshold to $a_{\text{crit}} \simeq 16.5$; and strong breaking ($\beta = 0.1$) significantly postpones it to $a_{\text{crit}} \simeq 21$. Surprisingly, stronger parity violation (small β) significantly delays the overtaking instability, with a_{crit} increasing from ~ 5 (GR) to ~ 21 for $\beta = 0.1$. This counterintuitive dynamical stabilization arises because the dCS scalar potential $\propto 1/(\beta r^6)$ becomes steeply repulsive at strong coupling, spatially expelling the scalar perturbation $\Theta(r)$ to larger radii. Consequently, the near-zone overlap between graviton and scalar modes, which mediates the non-Hermitian hybridization driving the instability, is dramatically suppressed, effectively shielding the gravitational mode against overtaking until the bump is pushed much farther out. This reveals a non-perturbative physical mechanism, symmetry breaking does not destabilize the system, but rather stabilizes the gravitational mode against the overtaking instability by a near-field resonance effect [44]. Stronger breaking enhances this stability, pushing the overtaking event to larger a . This non-trivial behavior, a profound dynamical consequence of breaking GR's isospectrality, echoes QNM threshold shifts induced by scalar hair in other modified gravity theories like Einstein-scalar-Gauss-Bonnet.

Fig. 3 depicts the real and imaginary parts of $\Delta\omega$ as functions of a . We focus on the post-overtaking stable regime with large a . For the real part $|\text{Re}(\Delta\omega)|$, the polar sector shows the largest deviation. As breaking increases, the offset is progressively suppressed, indicating the scalar coupling mitigates frequency shifts. Conversely, for the imaginary part $|\text{Im}(\Delta\omega)|$, an inversion pattern is observed, weak breaking exhibits the smallest offset, and it is close to the GR situation. As breaking strengthens, the damping offset significantly increases, with strong breaking showing the largest deviation. It reveals a dual effect of symmetry breaking,

1. On overtaking, strong breaking stabilizes the system, postponing a_{crit} ;
2. On asymptotic behavior, strong breaking makes the resulting stable mode more sensitive to perturbations in the potential's tail.

On the other hand, stronger coupling acts like a stiffer spring, making the spectrum more rigid against distant perturbations, while simultaneously opening a new channel for energy dissipation that sensitizes the damping rate to tail perturbations [45]. This mechanism, where energy is absorbed by the scalar field to alleviate damping, parallels the stabilization of overtones by scalar hair in Einstein-scalar-Gauss-Bonnet models [46]. Compared to the GR baseline, this asymmetric, β -dependent response dynamically quantifies the fingerprint of symmetry breaking.

Another entirely new phenomenon, scalar overtake, arises for $\beta = 1$ at small $a < 5$. Most strikingly, at

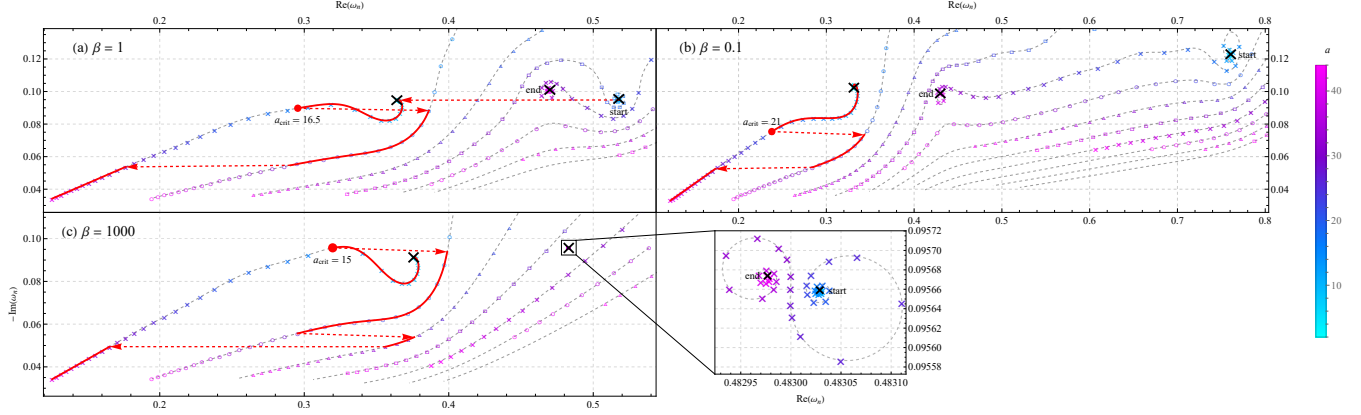


FIG. 1: QNM migration trajectories in the complex frequency plane for different symmetry-breaking strengths β .

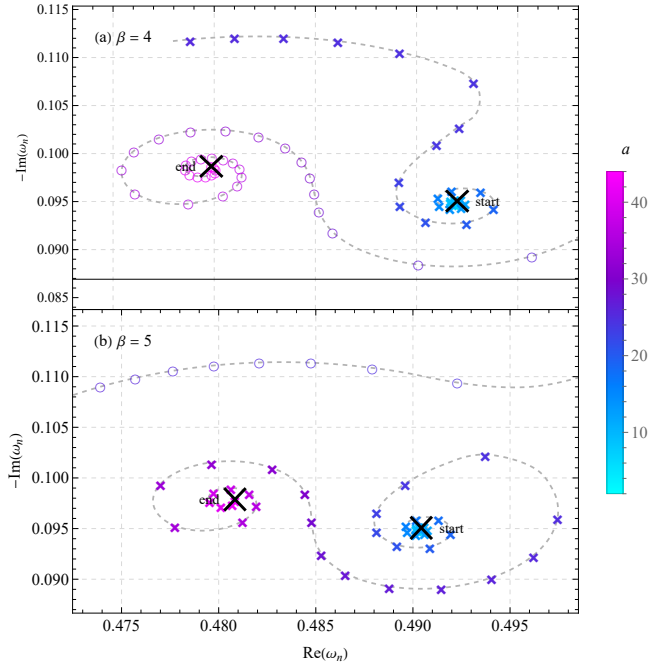


FIG. 2: Scalar mode migration trajectories in the complex frequency plane for $\beta = 4$ and 5 . It is manifest that the changes in the curves are discontinuous, i.e., curve merging occurs.

intermediate coupling ($\beta \simeq 1$) and near-peak bumps ($a \gtrsim 5$), the dCS pseudoscalar mode becomes impossible the globally least-damped (longest-lived) mode in the entire spectrum, a situation strictly impossible in general relativity (see red segments in panel(a) of Fig. 1 where the dominant-mode track ϖ abruptly switches to the scalar branch for $a \lesssim 5$). This will allow the pseudoscalar mode to dominate the late-time ringdown and may have an impact on the power-law tail of the time-domain signal, which could be detected by future gravitational wave detectors.

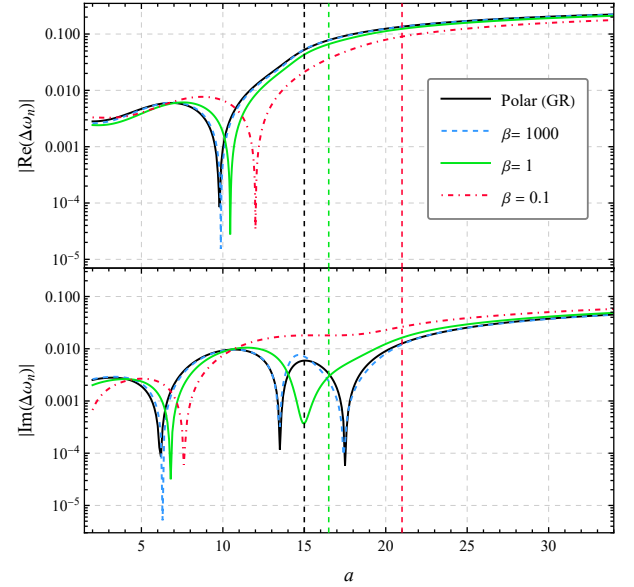


FIG. 3: The frequency deviation of the fundamental mode $\Delta\omega = \omega(\epsilon, a) - \omega(0)$ as a function of the bump position a , focusing on the post-overtaking stable regime ($a \gtrsim a_{\text{crit}}$).

In the intermediate coupling regime, the scalar mode overtake is physically driven by the non-Hermitian level repulsion. Utilizing the second-order perturbation theory to the effective Hamiltonian H_{eff} , the correction to the decay rate of scalar modes read

$$\text{Im}(\omega_s) \simeq \text{Im}(\omega_s^{\text{GR}}) + \text{Im} \left[\frac{\kappa_{sg}(\beta) \kappa_{gs}}{\Omega_s^2(\beta) - \Omega_g^2(a)} \right]. \quad (5)$$

This perturbative result elucidates the strict spatial selectivity of the phenomenon. The overtake is observed only for near-field bumps (small a) because the coupling integrals κ are dominated by short-range interaction terms $\sim r^{-5}$. Furthermore, the effect is suppressed at strong

symmetry breaking $\beta = 0.1$ because the stiffened dCS potential barrier spatially expels the scalar wavefunction, creating a spatial mismatch that quenches the effective coupling overlap despite the β^{-1} enhancement.

This scalar dominance, absent in GR or weak-breaking cases, represents a symmetry breaking induced, non-perturbative mode crossing. Here, the dCS pseudoscalar field ϕ invades and stabilizes the axial dynamics near the potential peak. The scalar mode gains enhanced longevity under near-peak bumps because of the strong chiral coupling. The complete absence of this overtake in the polar sector starkly highlights the selectivity of dCS breaking, it shatters the symmetry between parity sectors in GR and provides a diagnostic tool for parity violation in ringdown signals.

Conclusion and Discussion. In this Letter, we have introduced a novel diagnostic framework for probing symmetry breaking, using environment-driven spectral instabilities as a precision amplifier. Using dCS gravity as a paradigm for parity violation, we demonstrated a rich, non-perturbative phenomenology entirely absent in GR.

These findings have significant physical implications. The β -dependent critical threshold a_{crit} and the scalar overtake phenomenon transform weak, static spectral asymmetries into amplified dynamical signatures. For instance, under strong symmetry breaking, i.e., $\beta \sim 0.1$, the spectral topology is fundamentally reshaped in the stabilization window ($15 \lesssim a \lesssim 21$). However, the immediate time-domain signatures in this regime might be subtle, as the excitation factors of the theoretically least-damped modes can be sub-dominant during the early ringdown. Consequently, the initial waveforms of dCS and GR black holes may appear degenerate. Nevertheless, this degeneracy can be resolved by extracting the specific frequency of the asymptotic tail using future high-precision detectors, such as LISA or the Einstein Telescope. Detecting a “stabilized” fundamental frequency—in a parameter region where GR predicts a discrete frequency jump due to mode overtaking—would serve as a robust discriminator for parity violation. Crucially, as detailed in the SM, the critical instability point follows a logarithmic scaling with the perturbation amplitude ($a_{\text{crit}} \propto -\log \epsilon$). This implies that the spectral stabilization is a fundamental feature that persists even for astrophysically weak environmental perturbations, merely shifting the critical window to larger distances.

The extension of this framework to astrophysically ubiquitous Kerr black holes is a crucial next step. Rotation itself acts as a non-Hermitian parameter, lifting the m -mode degeneracy and potentially driving the spectrum toward EPs [31]. We anticipate a rich interplay between the dCS-induced symmetry breaking and the black hole spin a/M , leading to new topological phenomena. Future work should also distinguish the physical origins of

these phenomena, while topological reconnections naturally arise from generic non-Hermitian two-field couplings, the counterintuitive stabilization and scalar dominance appear to be specific dynamical signatures attributable to the parity-breaking mechanism.

This framework not only provides new avenues to constrain dCS gravity—potentially enabling tighter bounds on breaking parameters [13, 25, 47]—but also opens a general path to test fundamental symmetries using BH non-Hermitian dynamics, yielding detectable signatures in LIGO/Virgo or future LISA data and bridging theory with observational astrophysics and constraining beyond GR physics.

Acknowledgments. This work is supported in part by the National Key Research and Development Program of China No. 2020YFC2201501, in part by the National Natural Science Foundation of China No. 12475067 and No. 12235019. Moreover, C.Lan is supported by Yantai University under Grant No. WL22B224.

* huhanwen@itp.ac.cn

† stlanchen@126.com

‡ guozk@itp.ac.cn

- [1] T. Regge and J. A. Wheeler, Phys. Rev. **108**, 1063 (1957).
- [2] S. Chandrasekhar, Proc. Roy. Soc. Lond. A **343**, 289 (1975).
- [3] S. Chandrasekhar, *The mathematical theory of black holes* (Oxford university press, 1985).
- [4] K. D. Kokkotas and B. G. Schmidt, Living Rev. Rel. **2**, 2 (1999), arXiv:gr-qc/9909058.
- [5] E. Berti, V. Cardoso, and A. O. Starinets, Class. Quant. Grav. **26**, 163001 (2009), arXiv:0905.2975 [gr-qc].
- [6] C.-Y. Chen, M. Bouhmadi-López, and P. Chen, Eur. Phys. J. Plus **136**, 253 (2021), arXiv:2103.01249 [gr-qc].
- [7] D. Li, A. Hussain, P. Wagle, Y. Chen, N. Yunes, and A. Zimmerman, Phys. Rev. D **109**, 104026 (2024), arXiv:2310.06033 [gr-qc].
- [8] D. del Corral and J. Olmedo, Phys. Rev. D **105**, 064053 (2022), arXiv:2201.09584 [gr-qc].
- [9] N. Herceg, T. Jurić, A. N. Kumara, A. Samsarov, and I. Smolić, JHEP **05**, 083 (2025), arXiv:2409.01402 [gr-qc].
- [10] N. Herceg, T. Jurić, A. N. Kumara, A. Samsarov, and I. Smolić (2025) arXiv:2503.15181 [gr-qc].
- [11] A. K.-W. Chung, K. K.-H. Lam, and N. Yunes, Phys. Rev. D **111**, 124052 (2025), arXiv:2503.11759 [gr-qc].
- [12] K. Yagi and H. Yang, Phys. Rev. D **97**, 104018 (2018), arXiv:1712.00682 [gr-qc].
- [13] S. E. Perkins, R. Nair, H. O. Silva, and N. Yunes, Phys. Rev. D **104**, 024060 (2021), arXiv:2104.11189 [gr-qc].
- [14] M. Califano, R. D’Agostino, and D. Vernieri, Phys. Rev. D **109**, 104062 (2024), arXiv:2311.02161 [gr-qc].
- [15] T. Zhu, W. Zhao, J.-M. Yan, Y.-Z. Wang, C. Gong, and A. Wang, Phys. Rev. D **110**, 064044 (2024), arXiv:2304.09025 [gr-qc].
- [16] B.-Y. Zhang, T. Zhu, J.-M. Yan, J.-F. Zhang, and X. Zhang, Phys. Rev. D **111**, 104012 (2025), arXiv:2502.04776 [gr-qc].

- [17] S. P. Kim, J. Korean Phys. Soc. **49**, 764 (2006), arXiv:gr-qc/0512005.
 - [18] D. Areán, D. G. Fariña, and K. Landsteiner, JHEP **12**, 187 (2023), arXiv:2307.08751 [hep-th].
 - [19] J. Besson, J. Carballo, C. Pantelidou, and B. Withers, Front. in Phys. **13**, 1638583 (2025), arXiv:2507.16493 [gr-qc].
 - [20] P. T. Leung, Y. T. Liu, W. M. Suen, C. Y. Tam, and K. Young, Phys. Rev. Lett. **78**, 2894 (1997), arXiv:gr-qc/9903031.
 - [21] M. H.-Y. Cheung, K. Destounis, R. P. Macedo, E. Berti, and V. Cardoso, Phys. Rev. Lett. **128**, 111103 (2022), arXiv:2111.05415 [gr-qc].
 - [22] L. Solidoro, S. Patrick, S. Weinfurtner, and R. Gregory, Phys. Rev. Lett. **135**, 051401 (2025), arXiv:2406.11013 [gr-qc].
 - [23] S.-F. Shen, G.-R. Li, R. G. Daghigh, J. C. Morey, M. D. Green, W.-L. Qian, and R.-H. Yue, (2025), arXiv:2509.23372 [gr-qc].
 - [24] C. Molina, P. Pani, V. Cardoso, and L. Gualtieri, Phys. Rev. D **81**, 124021 (2010), arXiv:1004.4007 [gr-qc].
 - [25] P. Wagle, N. Yunes, and H. O. Silva, Phys. Rev. D **105**, 124003 (2022), arXiv:2103.09913 [gr-qc].
 - [26] M. Srivastava, Y. Chen, and S. Shankaranarayanan, Phys. Rev. D **104**, 064034 (2021), arXiv:2106.06209 [gr-qc].
 - [27] P. Wagle, D. Li, Y. Chen, and N. Yunes, Phys. Rev. D **109**, 104029 (2024), arXiv:2311.07706 [gr-qc].
 - [28] T. Alapati and S. Shankaranarayanan, Phys. Rev. D **112**, 024053 (2025), arXiv:2506.03600 [gr-qc].
 - [29] N. Yunes and F. Pretorius, Phys. Rev. D **79**, 084043 (2009), arXiv:0902.4669 [gr-qc].
 - [30] E. Berti *et al.*, (2025), arXiv:2505.23895 [gr-qc].
 - [31] J. P. Cavalcante, M. Richartz, and B. C. da Cunha, Phys. Rev. Lett. **133**, 261401 (2024), arXiv:2407.20850 [gr-qc].
 - [32] K.-i. Kubota and H. Motohashi, (2025), arXiv:2509.06411 [gr-qc].
 - [33] S. Klaiman, N. Moiseyev, and U. Gunther, Phys. Rev. Lett. **101**, 080402 (2008), arXiv:0802.2457 [quant-ph].
 - [34] J. Schnabel, H. Cartarius, J. Main, G. Wunner, and W. D. Heiss, Phys. Rev. A **95**, 053868 (2017), arXiv:1703.05091 [physics.optics].
 - [35] A. I. Nesterov and F. Aceves de la Cruz, J. Phys. A **41**, 485304 (2008), arXiv:0806.3720 [quant-ph].
 - [36] A. Kumar, K. W. Murch, and Y. N. Joglekar, Phys. Rev. A **105**, 012422 (2022), arXiv:2109.07503 [quant-ph].
 - [37] W. D. Heiss, J. Phys. A **45**, 444016 (2012), arXiv:1210.7536 [quant-ph].
 - [38] R. Oliveira, D. M. Dantas, and C. A. S. Almeida, EPL **135**, 10003 (2021), arXiv:2105.07956 [gr-qc].
 - [39] C. Zhang, A. Wang, and T. Zhu, Eur. Phys. J. C **83**, 841 (2023), arXiv:2209.04735 [gr-qc].
 - [40] W.-D. Guo, Q. Tan, and Y.-X. Liu, JCAP **07**, 008 (2024), arXiv:2312.16605 [gr-qc].
 - [41] S. Boudet, F. Bombacigno, G. J. Olmo, and P. J. Porfirio, JCAP **05**, 032 (2022), arXiv:2203.04000 [gr-qc].
 - [42] V. Cardoso, K. Destounis, F. Duque, R. P. Macedo, and A. Maselli, Phys. Rev. D **105**, L061501 (2022), arXiv:2109.00005 [gr-qc].
 - [43] V. Cardoso, K. Destounis, F. Duque, R. Panosso Macedo, and A. Maselli, Phys. Rev. Lett. **129**, 241103 (2022), arXiv:2210.01133 [gr-qc].
 - [44] M. Bojowald, E. I. Duque, and S. Shankaranarayanan, Phys. Rev. D **111**, 024051 (2025), arXiv:2410.17501 [gr-qc].
 - [45] S. Garcia-Saenz, G. Guo, P. Wang, and X. Wang, Phys. Rev. D **110**, 124045 (2024), arXiv:2409.13184 [gr-qc].
 - [46] G. Antoniou, A. Bakopoulos, and P. Kanti, Phys. Rev. D **97**, 084037 (2018), arXiv:1711.07431 [hep-th].
 - [47] H. O. Silva, A. M. Holgado, A. Cárdenas-Avendaño, and N. Yunes, Phys. Rev. Lett. **126**, 181101 (2021), arXiv:2004.01253 [gr-qc].
 - [48] Y. Yang, E. Berti, and N. Franchini, Phys. Rev. Lett. **135**, 201401 (2025), arXiv:2504.06072 [gr-qc].
-

SUPPLEMENTAL MATERIAL

Non-Hermitian perturbation theory for spectral dynamics. In this section, we establish a formal framework aimed at elucidating the physical mechanisms driving both the topological reconnection and the scalar mode overtake phenomena. We provide the detailed derivation of the effective 2×2 Hamiltonian and the resonance condition Eq. (4) presented in the main text. Since the critical overlap integrals depend non-trivially on both the breaking parameter β and the bump position a , this theory serves to predict the existence of EPs and spectral shifts qualitatively rather than determining their exact locations.

Technically, the perturbed wavefunction Φ evolves in an infinite-dimensional Hilbert space spanned by the complete set of unperturbed GR eigenmodes. However, the spectral instabilities of interest—such as curve merging and mode overtaking—arise from the strong resonant interaction between specific mode pairs. Justified by this spectral selectivity, we adopt the two-mode approximation, neglecting the off-resonant couplings to distant spectator modes and projecting the full operator onto the relevant subspace spanned by a specific gravitational mode $|\psi_g^{(n)}\rangle$ and a scalar mode $|\psi_s^{(k)}\rangle$.

Accordingly, we construct a non-Hermitian perturbation theory [37, 48] for the coupled master equations

$$\hat{\mathcal{L}}(\beta, a)\Phi = \omega^2\Phi. \quad (6)$$

By rewriting the coupled wave equations Eq. (2) into the matrix form, we identify the specific forms of these operators acting on the state vector $\Phi = (\Psi, \Theta)^T$. The diagonal unperturbed operators correspond to the standard Regge-Wheeler and scalar potentials in Schwarzschild spacetime

$$\hat{H}_g^{\text{GR}} \equiv -\frac{d^2}{dr_*^2} + f\left(\frac{l(l+1)}{r^2} - \frac{6M}{r^3}\right), \quad \hat{H}_s^{\text{GR}} \equiv -\frac{d^2}{dr_*^2} + f\left(\frac{l(l+1)}{r^2} + \frac{2M}{r^3}\right). \quad (7)$$

The off-diagonal operators capture the parity-violating mixing. Comparison with Eq. (2a) identifies the gravitational to scalar coupling $\hat{\mathcal{C}}_{gs} \equiv 6Mf/r^5$. Conversely, Eq. (2b) reveals that both the scalar to gravitational coupling and the dCS correction to the scalar potential carry a β^{-1} scaling, allowing us to factor out the symmetry breaking parameter

$$\hat{\mathcal{C}}_{sg} \equiv f\frac{(l+2)!}{(l-2)!}\frac{6M}{r^5}, \quad \hat{\mathcal{P}}_{\text{dCS}} \equiv f\frac{l(l+1)}{r^2}\frac{36M^2}{r^6}. \quad (8)$$

Substituting these operators into Eq. (6), we decompose the operator into a diagonal unperturbed part, a symmetry-breaking interaction $\hat{V}_{\text{dCS}}(\beta) \equiv \hat{\mathcal{P}}_{\text{dCS}}/\beta$, and an environmental perturbation $\hat{V}_{\text{bump}}(a)$

$$\hat{\mathcal{L}} = \begin{pmatrix} \hat{H}_g^{\text{GR}} & 0 \\ 0 & \hat{H}_s^{\text{GR}} \end{pmatrix} + \begin{pmatrix} \hat{V}_{\text{bump}}(a) & \hat{\mathcal{C}}_{gs} \\ \beta^{-1}\hat{\mathcal{C}}_{sg} & \beta^{-1}\hat{\mathcal{P}}_{\text{dCS}} \end{pmatrix}. \quad (9)$$

By projecting the operator onto the subspace of the unperturbed n -th gravitational mode $|\psi_g^{(n)}\rangle$ and k -th scalar mode $|\psi_s^{(k)}\rangle$, we derive the local effective Hamiltonian

$$H_{\text{eff}} = \begin{pmatrix} \Omega_g^2(a) & \kappa_{gs} \\ \kappa_{sg}(\beta) & \Omega_s^2(\beta) \end{pmatrix}. \quad (10)$$

Here, the diagonal elements capture the bare frequencies renormalized by their respective perturbations. The gravitational level explicitly depends on the bump position via the overlap integral

$$\Omega_g^2(a) \equiv \omega_{g,\text{GR}}^{(n)2} + \langle \psi_g^{(n)} | \hat{V}_{\text{bump}}(a) | \psi_g^{(n)} \rangle, \quad (11)$$

where the inner product is defined by the integration over the tortoise coordinate $\langle \psi_a | \hat{O} | \psi_b \rangle \equiv \int_{-\infty}^{+\infty} dr_* \psi_a(r_*) \hat{O}(r_*) \psi_b(r_*)$, utilizing the unconjugated form appropriate for non-Hermitian QNM theory [20]. The scalar level describes the continuous spectral shift driven by the dCS potential

$$\Omega_s^2(\beta) \equiv \omega_{s,\text{GR}}^{(k)2} + \frac{1}{\beta} \langle \psi_s^{(k)} | \hat{\mathcal{P}}_{\text{dCS}} | \psi_s^{(k)} \rangle. \quad (12)$$

The off-diagonal terms represent the effective non-Hermitian couplings

$$\kappa_{gs} \equiv \langle \psi_g^{(n)} | \hat{\mathcal{C}}_{gs} | \psi_s^{(k)} \rangle, \quad \kappa_{sg}(\beta) \equiv \frac{1}{\beta} \langle \psi_s^{(k)} | \hat{\mathcal{C}}_{sg} | \psi_g^{(n)} \rangle. \quad (13)$$

The spectral topology is governed by the discriminant \mathcal{D} of the characteristic polynomial $\det(H_{\text{eff}} - \lambda \mathbf{I}) = 0$. Condition $\mathcal{D} = 0$ defines the locus of EPs in the parameter space

$$\mathcal{D}(\beta, a) = [\Omega_g^2(a) - \Omega_s^2(\beta)]^2 + 4\kappa_{gs}\kappa_{sg}(\beta) = 0. \quad (14)$$

This algebraic constraint implies that for a specific mode pair (n, k) , the reconnection event is strictly confined to a unique trajectory in the (β, a) parameter space. It necessitates that the squared frequency detuning, $\Omega_g^2(a) - \Omega_s^2(\beta)$, be exactly balanced by the non-Hermitian effective coupling product. This mechanism elucidates why varying the control parameter β drives the system through topological reconnections, as it continuously tunes the scalar sector into critical resonance with the gravitational spectrum.

Beyond the critical point, the same effective Hamiltonian explains the scalar mode overtake phenomenon observed at intermediate couplings. To quantify this, we apply second-order perturbation theory to H_{eff} in the non-degenerate limit. By treating the off-diagonal coupling terms as perturbations to the diagonal bare frequencies, the shift in the complex eigenvalue of the scalar mode $\lambda_s = \omega_s^2$ is derived as

$$\Delta\omega_s^2 \simeq \frac{H_{21}H_{12}}{H_{22} - H_{11}} = \frac{\kappa_{sg}(\beta)\kappa_{gs}}{\Omega_s^2(\beta) - \Omega_g^2(a)}. \quad (15)$$

Taking the imaginary part yields the decay rate as shown in the Eq. (5) of main text.

Scaling law of a_{crit} with perturbation amplitude ϵ . To validate the generality of the perturbation amplitude $\epsilon = 10^{-2}$ used in the main text chosen for numerical tractability, and to exclude the possibility that the observed critical phenomenon is an artifact of this large ϵ value, we here investigate the scaling relation of a_{crit} with ϵ . We track a_{crit} for the baseline GR polar mode as ϵ is varied from 10^{-2} down to 10^{-5} .

Our numerical results for $\beta = 1$ situation, as shown in Tab. I, clearly demonstrate a robust trend, as the perturbation amplitude ϵ decreases, the critical position a_{crit} is systematically pushed to larger distances. Despite minor numerical fluctuations at intermediate data points, the data exhibits a strong linear relationship on a semi-log plot.

TABLE I: Scaling relation data for the critical position a_{crit} as a function of the bump amplitude ϵ .

ϵ	10^{-2}	$10^{-2.5}$	10^{-3}	$10^{-3.5}$	10^{-4}	$10^{-4.5}$	10^{-5}
a_{crit}	16.5	27	25	34.5	33.5	43	42.5

A linear fit to the data a_{crit} vs. $\log(\epsilon)$ yields a high goodness-of-fit with $R^2 \simeq 0.91$, as shown in Fig. 4. This result robustly confirms our central argument, mode overtaking is a physical phenomenon that persists for arbitrarily small perturbations. For physically plausible, small ϵ , the critical point a_{crit} is pushed to very large distances, corroborating our claim in the main text that the critical phenomena are pushed to numerically challenging large distances.

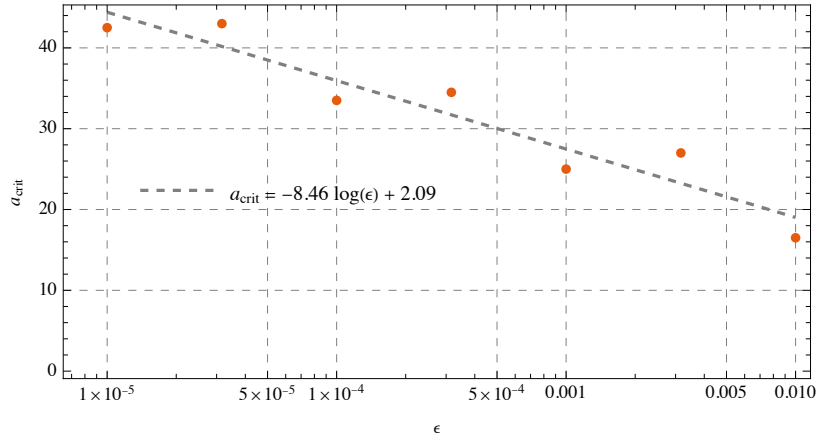


FIG. 4: Scaling relation of the critical position a_{crit} as a function of the perturbation amplitude ϵ , shown for the dCS axial mode with $\beta = 1$. The orange data points (from Tab. I) track the value of a_{crit} as ϵ is varied. The gray dashed line represents the linear fit $a_{\text{crit}} = -8.46 \log(\epsilon) + 2.09$. As the perturbation ϵ decreases to smaller, the critical point a_{crit} is systematically pushed to larger distances.